Journal of The Electrochemical Society, **146** (7) 2387-2392 (1999)
S0013-4651(98)09-048-X CCC: $7.00 © The Electrochemical Society, Inc.

In Situ X-Ray Absorption Spectroscopy Characterization of V_2O_5 Xerogel Cathodes upon Lithium Intercalation

Marco Giorgetti,[a,*] Stefano Passerini,[a,] William H. Smyrl,[a,***] Sanjeev Mukerjee,[b,**] X. Q. Yang,[b,**] and James McBreen[b,**]**

[a]*Corrosion Research Center, Department of Chemical Engineering and Materials Science, University of Minnesota, Minneapolis, Minnesota 55455, USA*
[b]*Department of Applied Science, Materials Science Division, Brookhaven National Laboratory, Upton, New York 11973, USA*

Vanadium pentoxide materials prepared through sol-gel processes act as excellent intercalation hosts for lithium as well as for polyvalent cations. Previous ex situ X-ray absorption spectroscopy and X-ray diffraction characterizations have shown that the electrochemical performance of vanadium pentoxide xerogels depends inversely on the long-range order of the V_2O_5-layered structure. Recently, new ways to prevent the self-organization of the dry materials, which takes place upon water removal from the starting hydrogel, have been introduced. In the present paper we report on the in situ X-ray absorption spectroscopy characterization of a spray-coated V_2O_5 (freeze-dried) xerogel cathode upon lithium intercalation.

Manuscript submitted September 11, 1998; revised manuscript received February 18, 1999.

The electrochemical properties of vanadium oxide electrodes prepared by sol-gel processes have been shown to depend on the structural and morphological characteristics that are in turn largely determined by the method of preparation. Previous studies have demonstrated that the morphology of thin-film vanadium oxide xerogels can be changed by changing the rate and mode of drying the starting hydrogel.[1-3] The resulting materials have intercalation capacities as high as 650 Ah/kg with corresponding specific energies exceeding 1600 Wh/kg. The preparation of vanadium pentoxide via sol-gel processing has been extensively reported and a comprehensive review is available.[4] Several papers focused on the hydrogel[4-8] have led to a more complete understanding of the chemistry of the process. Formation of hydrogels involves a gelation step that proceeds through formation of decavanadic acid and subsequent polycondensation.[5] The polycondensed vanadium oxyhydroxide material that precipitates and forms the gel has the characteristic shape of ribbons. The structure of the ribbons remains controversial. Two different models have been proposed for the layered structure of gel-based V_2O_5 materials. The older one, proposed by Legendre et al.,[9] was directly derived from the structure of crystalline V_2O_5. The second model, introduced by Yao et al.,[10] proposes that each V_2O_5 layer is constituted of two facing $VO_{1.5}$ sheets, further sandwiched by two layers of apical oxygens (one oxygen in each layer). Unfortunately, both structural models are characterized by the same X-ray diffraction pattern. Although the second model appears to give a more accurate estimation of the material density,[10] some uncertainty on the gel-based V_2O_5 structure remains. Nevertheless, both models predict the presence of coplanar apical oxygens on each side of the layers and in approximately similar positions.

Drying the V_2O_5 hydrogel, i.e., removing the water, results in ribbon stacking along the *c* direction. Such materials, named vanadium oxide xerogels (XRG), have also been characterized.[11-15] Slowly dried V_2O_5 xerogels are strongly anisotropic with a highly ordered layered structure characterized by a large basal separation distance. (8.75 Å) The reduced layer-layer interaction that results is responsible for the ability of V_2O_5 xerogels to reversibly expand upon intercalation, which causes the insertion process to be more reversible than in crystalline V_2O_5. In situ X-ray absorption spectroscopy (XAS) investigation on the latter material upon lithium insertion[16] has shown that a structural stress develops in vanadium oxide upon lithium intercalation. This restricts the reversible intercalation capacity to 0.78 equiv Li/mol V_2O_5. Insertion of lithium above this limit causes an irreversible phase transition. On the contrary, Baddour et al.[13] reported on the reversible insertion of up to 1 equiv Li/mol in dip-coated V_2O_5 xerogel electrodes. Higher insertion capacity was reported by West et al.,[15] who found that 1.6 equiv Li was reversibly inserted and removed for more than 40 cycles. Recently, it was shown[14,17] that V_2O_5 xerogel thin films were able to insert up to 3 or 4 equiv Li, respectively, under kinetic or thermodynamic conditions. The films were obtained by spin coating the hydrogel on an appropriate substrate. The excellent performance is due to the highly amorphous character of the xerogel and to the low anisotropy of the material resulting from the spin-coating process.[2] The incentive to improve the performance of V_2O_5 xerogel powders further led us to modify the drying procedure for bulk materials. In previous work, carbon powder was added in the early stages of the vanadium oxide gelation. The presence of carbon particles reduced the self-aggregation of the vanadium oxide ribbons in solution, and this induced morphological and structural changes in the final dried material. Electrochemical and XAS characterizations were used to correlate the lithium intercalation properties with the changes in the short-range order of the V_2O_5 xerogels.[18] The XAS experiments were performed ex situ on chemically lithiated xerogels. More recently, experimental setups that allow in situ XAS measurements on complete electrochemical cells have been developed.[19,20] The possibility of an in situ verification of the correlation between the electrochemical performance and the short-range structure of V_2O_5 xerogels has stimulated the work reported in the present study.

Experimental

Vanadium oxide xerogels were prepared by a sol-gel route described elsewhere.[2,4] A 0.5 M solution of sodium metavanadate (Fluka, >98%) was eluted through a column loaded with a proton-exchange resin (Dowex 50 WX_2 50-100 mesh). The effluent, a pale yellow solution of decavanadic acid, was collected in glass containers. One day aging with no agitation was sufficient to obtain a mature homogeneous vanadium oxide hydrogel.

Dried xerogel was obtained by freeze-drying the hydrogel under vacuum. In order to obtain a high surface area, the experimental setup consisted of a large container attached to a high-volume pumping rate vacuum pump. After about 120 h in the freeze dryer, the sample was transferred into a vacuum oven for the final drying step (12 h at 100°C and 10^{-3} Torr). With this procedure, the pore water and physically bound water[18,21] was completely removed. The resulting red powder of V_2O_5 xerogel contained only the strongly bonded water, 0.5 mol H_2O per mol V_2O_5. The powder was then ballmilled and sieved (400 mesh) prior to any further use.

V_2O_5 xerogel cathodes were prepared by spray coating onto 25 μm thick aluminum foils. The details of the procedure are given elsewhere.[21] The composition of the spray-coated electrodes was

* Electrochemical Society Student Member.
** Electrochemical Society Active Member.
*** Electrochemicqal Society Fellow.

S0013-4651(98)09-048-X CCC: $7.00

80% V_2O_5 xerogel, 10% polyvinylidene fluoride (PVDF) binder (Kynar, ELF Atochem), and 10% carbon (Ketjen black, Akzo Nobel). The active material loading ranged from 2 to 4 mg/cm^2.

The xerogel powders as well as the spray-coated cathodes were highly hygroscopic so that special precautions were required for preparing and handling the samples as well as for assembling the cells. In particular, the exposure to ambient (humid) air was avoided by handling all materials and cells in a dry room (University of Minnesota) or in a dry box (Brookhaven National Laboratory).

The electrochemical characterization of the spray-coated electrodes was performed in a coin cell assembly. Spray-coated samples were cut in the form of disks for the cathodes (16.2 mm diam). Lithium disks were used as anodes. Two layers of separator (Celgard, Hoechst Celanese), impregnated with the electrolyte, were used to separate the cathode and the anode in the coin cells. The electrolyte was a 1 M solution of $LiClO_4$ (Fluka, high-purity dried at 170°C under vacuum) in (1:1) propylene carbonate:ethylene carbonate (PC:EC, Grant Chemicals, high-purity, $H_2O < 20$ ppm). Galvanostatic charge/discharge tests were performed using a battery cycler (Arbin Instruments, College Station, Texas). The discharge rates (C/n) reported in this work (later called actual rates) are given on the basis of the actual discharge time. The actual rate that corresponds to a selected discharge current is taken as the inverse of the actual discharge time (n).

A special spectroelectrochemical cell was used to perform in situ XAS experiments. The details of the cell are given elsewhere.[20] The cell arrangement consisted of sandwiching a spray-coated V_2O_5 xerogel cathode disk (19.05 mm diam), two layers of electrolyte-impregnated separator, and a lithium anode. The same electrochemically active components (cathode, anode, separator, and electrolyte) described earlier were used to assemble the spectroelectrochemical cell. Two identical cells were used for the in situ XAS characterization of V_2O_5 xerogel cathodes as a function of the state of lithium insertion level. This allowed us to acquire two distinct series of XAS spectra in which the amount of lithium inserted in the active material was either increased or lowered. The lithium insertion level in the two cathodes was changed by applying a constant current to the cells, cathodic or anodic, respectively. To perform the in situ XAS experiments upon the series of decreasing amounts of inserted lithium, one electrode was preintercalated with about 1.5 equiv of Li^+/mol active material. The two cells were run alternatively, providing at least 20 min of relaxation time before taking the XAS spectra. A summary of the discharged and charged electrodes that includes the lithium composition in the active material, the formal oxidation state of vanadium, and the electrode open-circuit (OC) voltage is given in Table I.

The X-ray absorption experiments were conducted at the National Synchrotron Light Source (NSLS) using the beam line X11 A operating at 2.5 GeV and a typical current of 310 mA. The details pertaining to the design of the monochromator, resolution, and detune procedure are given elsewhere.[19] Harmonics were rejected by detuning (50%). Data were acquired at the V K-edge in the transmission mode. Ionization chambers were used to measure the incident (I_o) and the transmitted (I_t) radiation intensities. A third chamber (I_r) was used in conjunction with a standard vanadium foil as reference. This provided an internal calibration for the alignment of the edge position. A mixture of 90% He and 10% N_2 was used in the I_o ionization chamber, while pure nitrogen was used in the I_t and I_r detectors. X-ray absorption near-edge structure (XANES) spectra were taken every 0.5 to 50 eV after the edge with an integration time of 1 s. Extended X-ray absorption spectroscopy (EXAFS) spectra were collected up to $\mathbf{k} = 18$ every 0.05 $\mathbf{k}$ with a 3 s integration time.

The XANES spectra were normalized to an edge jump of unity after removal of the background absorption by subtraction of a linear function extrapolated from the pre-edge region and of a third-order polynomial (spline) function from the post-edge region. The vanadium K-edge energy position of the material under study as well as the standard materials were taken at $\mu x = 0.5$. This was performed to avoid uncertainties associated with the pre-edge peaks in the spectrum of vanadium oxides.

The oxidation state of vanadium as a function of the amount of lithium inserted in the V_2O_5 xerogel cathodes was monitored by referring to a (pre-edge position) and (K-edge position) vs. (oxidation state) standard curve. The standard curves, illustrated in Fig. 1, were determined by plotting the vanadium pre-edge and K-edge energy positions of common vanadium oxide standards (VO, VO_2, and crystalline V_2O_5). The standard curve is in good agreement with the previous work of Wong et al.[22]

Results

Figure 2 shows the behavior of a spray-coated V_2O_5 xerogel electrode (also called sc-XRG) upon galvanostatic charge/discharge cycles. The lithium insertion and release processes were driven at the same current ($I = 0.065$ mA; $J = 0.034$ mA/cm^2), which corresponded to a rate of C/12 (12 h discharge). The cycles were operated between 1.5 and 4.0 V. The electrode voltage behavior upon discharge, shown in Fig. 2, is typical of low-ordered, V_2O_5 xerogel materials.[18,23-25] With the exception of the final part of the discharge (>10 h), the curve shape is almost featureless with a smooth voltage change over the entire intercalation range.

The comparison of the discharge curves (first, second, and a generic one) reported in Fig. 2 shows only small differences upon cycling, both in terms of voltage curve shape and in the amount of lithium intercalated. The first modification is attributable to the lower open-circuit potential (OCP) of the pristine material (as coat-

Table I. Summary of the charged and discharged electrodes used for the in situ XAS experiments. The lithium insertion level in the two electrodes was changed by applying constant current pulses (+0.55 mA) for selected amounts of time. The formal oxidation state of vanadium has been calculated by combining the results of the chemical analysis and the coulometric experiment.

Discharged electrode				Charged electrode			
Step	$Li_xV_2O_5$ x (±0.01)	Formal oxidation state of V (±0.005)	OCV (V) (±0.001)	Step	$Li_xV_2O_5$ x (±0.01)	Formal oxidation state of V (±0.005)	OCV (V) (±0.001)
0	0.00	+5.00	3.790	0	1.47	+4.26	2.554
1	0.29	+4.85	3.352	1	1.28	+4.36	2.670
2	0.58	+4.71	3.143	2	1.10	+4.45	2.690
3	0.87	+4.56	2.801	3	0.98	+4.51	2.777
4	1.05	+4.47	2.658	4	0.80	+4.60	3.040
5	1.23	+4.36	2.533	5	0.62	+4.69	3.128
6	1.33	+4.33	2.538	6	0.54	+4.73	3.290
7	1.60	+4.20	2.390	7	0.37	+4.82	3.341
8	1.88	+4.06	2.200	8	0.09	+4.95	3.760
9	2.46	+3.77	1.760				

S0013-4651(98)09-048-X CCC: $7.00 © The Electrochemical Society, Inc.

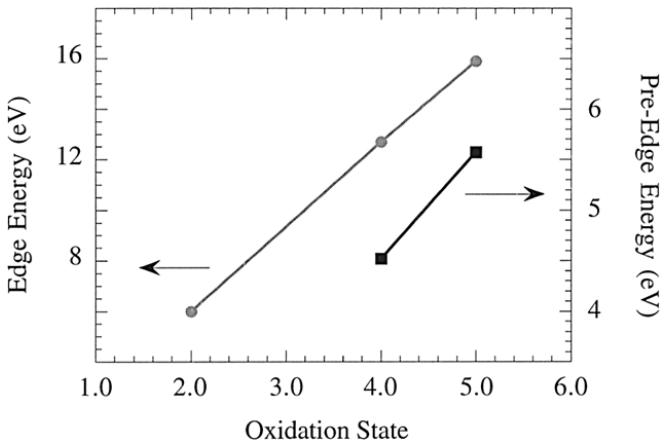

Figure 1. K-edge position (●, left axis) and pre-edge peak position (■, right axis) vs. (oxidation state) calibration curve of common vanadium oxide standards (VO, VO_2, and crystalline V_2O_5). The K-edge position was determined as described in the Experimental section.

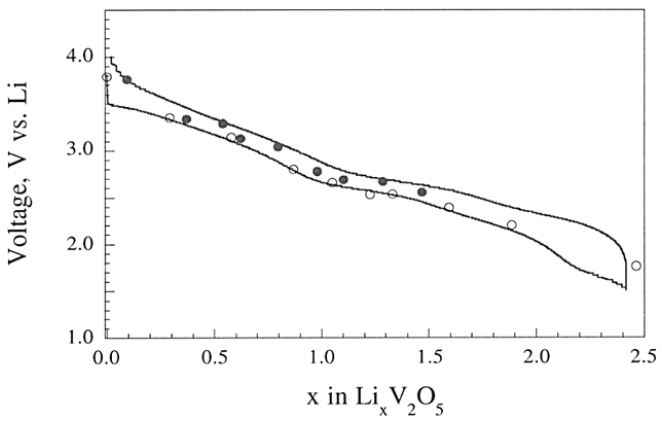

Figure 3. Voltage behavior of a spray-coated V_2O_5 xerogel electrode in coin cell (2016) assembly during a galvanostatic charge/discharge cycle (I = 0.02 mA). Electrode area: 2.06 cm^2. Active material mass loading: 3.08 mg (1.49 mg/cm^2). Anode: lithium. Separator: two layers of Celgard. Electrolyte: 1 M $LiClO_4$ in EC:PC (1:1). Room temperature.

ed). Most likely, this was due to a partial reduction of the active material induced by the addition of a solvent in the spray-coating procedure. In addition, the rest period between a charge and the following discharge was limited to only 15 min. A residual, uneven lithium distribution within the active material particles can also contribute to the higher initial voltage seen in the subsequent discharges. A slight decrease of capacity upon cycling is also shown in Fig. 2. The first cycle capacity was above 290 mAh/g of active material. It decreased to 280 mAh/g at the second cycle and to a stable value of 270 mAh/g upon continuous cycling.

Figure 3 shows the voltage behavior of a sc-XRG electrode during the first lithium insertion and release cycle. The experiment was performed with a low charge and discharge current (I = 0.02 mA; J = 0.0097 mA/cm^2), which corresponded to an actual rate of C/55 (discharge time: 55 h). The cell was cycled between the voltage cutoff limits of 1.5 and 4.0 V, respectively. In this condition, the spray-coated cathode was able to intercalate more than 2.4 Li^+/mol active material, which corresponds to a capacity of 340 mAh/g. The test was performed at a low rate to obtain a quasi-equilibrium voltage vs. composition curve of the sc-XRG cathode. With the exception of the initial and final part (where the cell polarization is high), the voltage hysteresis between the discharge and the charge curve is below 200 mV.

In Fig. 3 are also shown the OCPs of the two cells used in the in situ XAS experiments (also reported in Table I). The data points for the insertion cell (○) and the release cell (●) fell inside the charge and discharge curves. This experimental evidence indicates that the sc-XRG electrodes in the spectroelectrochemical cells used for the XAS experiments performed as well as in standard coin cell assemblies.

In situ XANES of the spray-coated V_2O_5 xerogels as a function of the lithium content were taken at the vanadium K-edge. The spectra were recorded for two cells for increasing (Fig. 4A, discharged cell) and decreasing (Fig. 4B, charged cell) amounts of inserted lithium. The lithium compositions at which the XAS spectra were taken on the two cells (discharged and charged) are given in Table I and in Fig. 3. For clarity, only a few selected spectra of the two cells are reported in Fig. 4 (the lithium compositions are indicated in the figure).

Both series of XANES spectra show similar changes of the major features for different levels of lithium insertion, clearly indicating the reversibility of the lithium insertion process in the freeze-dried V_2O_5 xerogel.

The first feature seen in the spectra is the pre-edge peak (labeled a in Fig. 4). This feature is typical of vanadium oxides and is associated with dipole forbidden $s \rightarrow d$ transitions that become allowed in nonoctahedral symmetry as the vanadium 3d states mix with the oxygen p states. Therefore, the intensity of the pre-edge peak is proportional to the deviation from octahedral symmetry of the vanadium site.[18,22] The pre-edge peak is seen to decrease in intensity and to shift toward lower energy with increasing amounts of inserted lithium.

The second and the third features, called the edge and the edge resonance (b), are related to the energy absorption by core electrons.

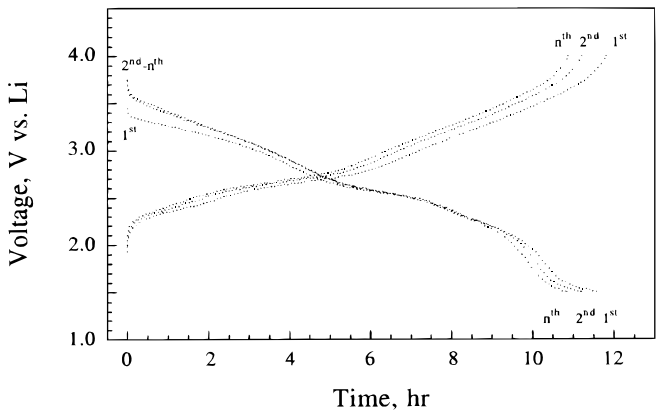

Figure 2. Galvanostatic charge/discharge cycles of a spray-coated V_2O_5 xerogel electrode in coin cell (2016) assembly. Charge and discharge current: 0.065 mA. Electrode area: 2.06 cm^2. Active material mass loading: 4.05 mg (1.97 mg/cm^2). Anode: lithium. Separator: two layers of Celgard. Electrolyte: 1 M $LiClO_4$ in EC:PC (1:1). Room temperature.

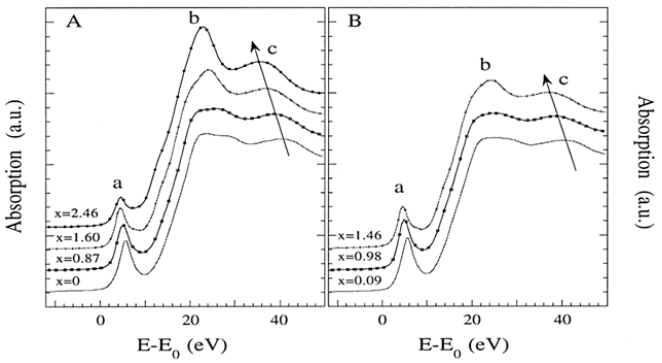

Figure 4. Selected XANES spectra recorded at the vanadium K-edge of a spray-coated V_2O_5 xerogel electrode (A) upon lithium insertion and (B) release. The lithium compositions (x in $Li_xV_2O_5$) are indicated in the figure. The energy scale is referred to the K-edge of pure vanadium (E_o = 5465 eV).

S0013-4651(98)09-048-X CCC: $7.00

These features are sensitive to the effective oxidation state of the vanadium (energy position of the edge) and the chemical environment surrounding the vanadium site. In accord with the pre-edge peak, the edge position is also seen to shift toward lower energy for increasing amounts of inserted lithium.

The spectra reported in Fig. 4 show major changes in both the intensity and the shape of the edge resonance. In particular, the shape changed from two well-defined peaks to a single peak upon lithium insertion. A similar behavior of the edge resonance was observed by Stallworth et al.[26] in crystalline V_6O_{13}. The edge resonance is associated with the continuum and is due to multiple scattering resonances of the photoelectrons.[27,28] V_2O_5 gel-based materials are formed of distorted, square-based [VO_5] pyramids with four basal and one apical oxygens. Previous calculations by Stizza et al.[29,30] have shown that the intensity and the shape of the edge resonance are affected by the symmetry of the four basal oxygens surrounding the vanadium sites.

The last feature seen in Fig. 4 (labeled c) is the first EXAFS oscillation that gives information about the average positions of the first-shell atoms surrounding the vanadium.[26,31,32] The relative position of the first EXAFS oscillation moves toward lower energy as the amount of inserted lithium is increased as indicated by the arrow in the figure.

In conjunction with the XANES measurements, EXAFS spectra were also recorded. Figure 5 shows the behavior of the **k**-weighted EXAFS signals for increasing (A, discharged cell) and decreasing (B, charged cell) amounts of inserted lithium. Despite the difficulties introduced by the experimental setup for the in situ measurements, the spectra showed a very low noise-to-signal ratio, even at high values of the wave vector **k** (>13 $Å^{-1}$).

The two series of spectra are characterized by a general loss of features upon increasing the lithium insertion level. The spectra taken at the highest lithium insertion level show a single damped oscillation that can be associated with a quasi-homogeneous first shell around the vanadium site.

Discussion

The results of the electrochemical characterization illustrated in Fig. 2 and 3 show the behavior of the freeze-dried V_2O_5 xerogel as a host for lithium intercalation. The material was able to reversibly intercalate about 2 equiv Li/mol V_2O_5 in 12 h discharges (C/12). At lower insertion rates (C/55) the insertion capacity was above 2.4 Li^+ per mol active material. In previous work[18] based on the ex situ XAS characterization of chemically lithiated V_2O_5 xerogels, it was shown that the insertion capacity of the materials was enhanced by the addition of carbon particles in early stages of the hydrogel formation. The resulting materials were characterized by a lower domain size and with less order of the layered structure due to the reduction of the spontaneous stacking of V_2O_5 ribbons upon water removal from the hydrogel to form the xerogel. This allowed faster rates and larger capacity of lithium intercalation in the carbon-added xerogels. In the V_2O_5 xerogel studied in the present work, the water was removed by freeze-drying the hydrogel. Therefore, at an early stage the hydrogel freezes and this reduces the self-organization of the solid phase as water is removed. The resulting material is characterized by an extremely low-ordered structure, which makes it difficult to carry out further characterization by means, for example, of X-ray diffraction.

Recently, in situ XAS characterization facilities have been developed which allow one to obtain useful information on the short-range order modifications that take place upon lithium insertion. The experiments in the present study were performed on complete electrochemical cells that made the interpretation of the measurements more complete than our previous ex situ measurements but that agree with the previous study.[18] Figures 6 and 7 illustrate the behavior of the features seen in the XANES spectra reported in Fig. 4. The energy position of the pre-edge peak and the edge as a function of the lithium composition is shown in Fig. 6. As seen in the figure, the experimental data points obtained upon lithium insertion and release are very close. This evidence clearly indicates that the freeze-dried V_2O_5 xerogel upon lithium intercalation has complete electronic reversibility.

All sets of data shown in Fig. 6 follow a straight-line behavior as a function of the lithium content. The linear fits, indicated by the solid lines in the figure, are obtained over both sets of data (charged and discharged electrodes). The slight scatter of the data is within the experimental error for the selected energy step (0.5 eV). Both features, the pre-edge peak and the edge, showed a shift toward lower energy for increasing amounts of intercalated lithium. As expected, the shift of the edge is more marked since it involves multiple scattering resonances that depend on the interatomic distances and the coordination geometry.[33] On the other hand, the pre-edge peak

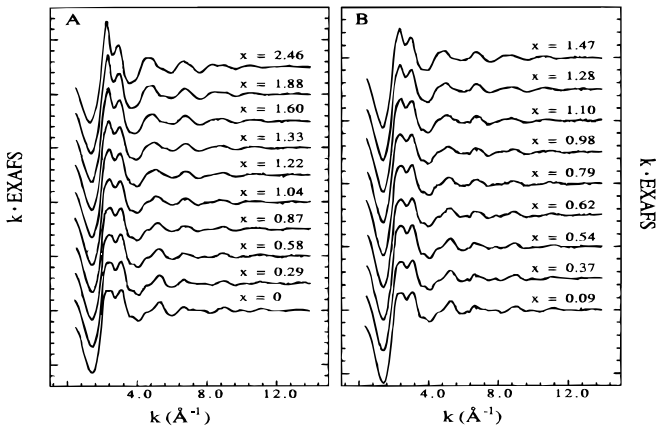

Figure 5. K-weighted EXAFS curves at the vanadium K-edge of spray-coated V_2O_5 xerogel electrodes upon (A) lithium insertion and (B) release. The lithium compositions (x in $Li_xV_2O_5$) are indicated in the figure.

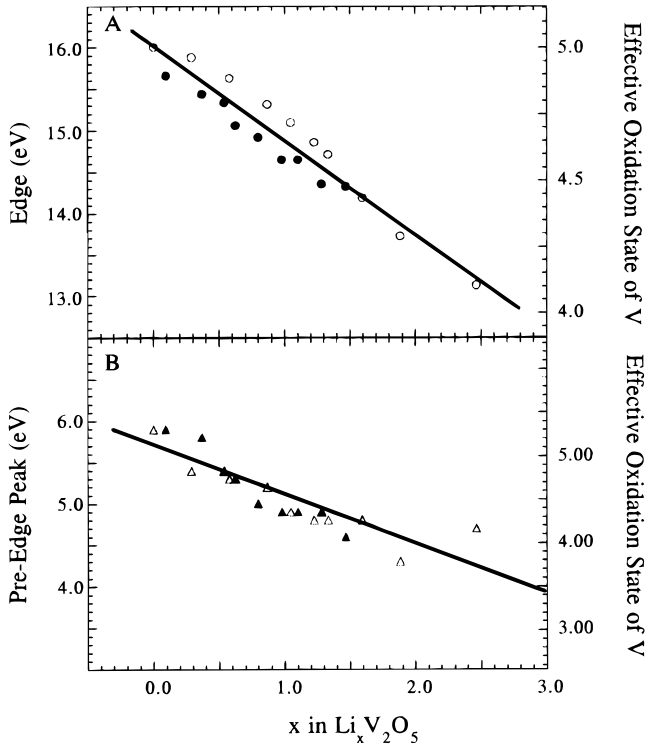

Figure 6. XANES pre-edge peak (▲, △) and edge shifts (●, ○) as a function of Li composition in spray-coated V_2O_5 xerogel. The data were extracted from the two sets of measurements, some of which are shown in Fig. 4. The edge shifts were taken at $\mu x = 0.5$. Further details are given in the Experimental section. Empty markers refer to the set of measurements taken upon increasing Li insertion levels. Solid markers refer to the set of lithium-release measurements.

S0013-4651(98)09-048-X CCC: $7.00 © The Electrochemical Society, Inc.

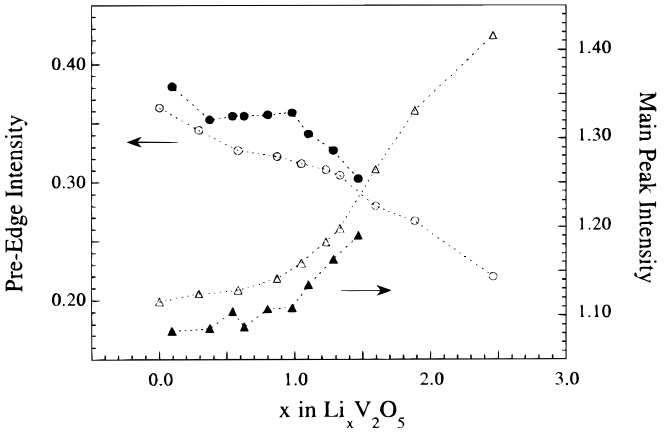

Figure 7. XANES pre-edge peak (●, ○) and main peak (▲, △) intensities as a function of the lithium composition in spray-coated V_2O_5 xerogel. The data were extracted from the two sets of measurements, some of which are shown in Fig. 4. Empty markers refer to the set of measurements taken upon increasing lithium insertion levels. Solid markers refer to the set of lithium-release measurements.

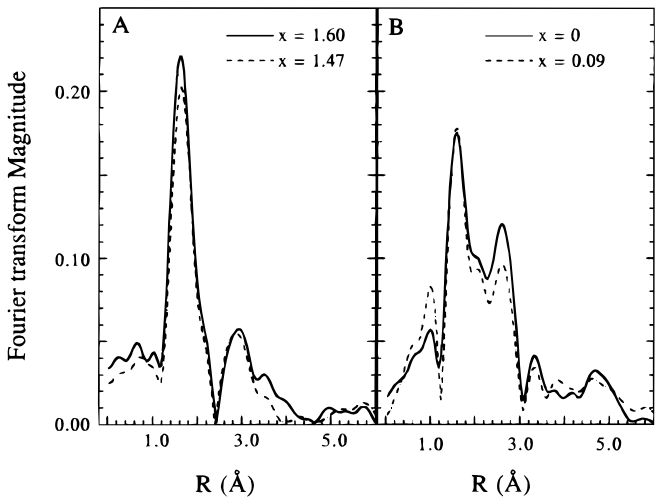

Figure 8. Comparison of the FT curves obtained from two different spray-coated V_2O_5 xerogel electrodes at similar lithium insertion levels (A) $x \approx 1.5$ and (B) $x \approx 0$, during the lithium (—) insertion and (- - -) release. $\Delta k = 3.4$-13.5. **k**-weighted.

involves electronic transitions to a bound state; then it provides a better indicator of the formal oxidation state. An estimation of the effective oxidation state was performed by using the pre-edge peak and the K-edge shifts of the vanadium standard compounds (see Fig. 1) as reference (right axis of A and B in Fig. 6). The results agreed fairly well. The effective oxidation state of the vanadium upon lithium insertion was calculated to reach a minimum of +4.0 when calculated from the pre-edge peak shift and of +4.1 when calculated from the edge shift. These results do not fully agree with the formal oxidation state (+3.75, see Table I) as obtained from the results of the chemical analysis performed on the samples used for the electrochemical tests. We conclude that a fraction of the negative charge is delocalized over the structure. A similar but even larger effect was seen previously in lithiated V_2O_5 aerogels.[34]

The XANES spectra reported in Fig. 4 show changes in intensity of both the pre-edge as well as the main peak, which indicate changes in the overall symmetry of the vanadium site. The pre-edge peak shows major changes in intensity as a function of the amount of the inserted lithium (Fig. 7). The linear decrease indicates a reduction of the distortion of the VO_5 square pyramid originally present in xerogel[18] as well as crystalline V_2O_5.[22] The resultant increase of the symmetry around the vanadium site upon lithium insertion is also indicated by an increase in magnitude of the edge resonance (Fig. 7). As discussed earlier, the intensity of the edge resonance (peak b in Fig. 4) is directly correlated to the symmetry of the basal oxygen configuration around the vanadium site. Once more, the bonding modifications revealed by the XANES measurements upon lithium insertion appear to be reversible. In fact, all the features seen in the XANES spectrum of the charged electrode when most of the lithium was removed ($x = 0.09$) appears to be extremely close to those of the pristine material.

Summarizing, the analysis of the XANES measurements reveals electronic and structural reversibility of the material upon lithium intercalation, at least for 1.5 equiv Li/mol active material. Such reversibility is also shown by a qualitative analysis of the EXAFS measurements. In Fig. 8 are shown the Fourier transform (FT) plots of the discharged and charged electrodes at similar lithium insertion levels. The most intense peak, which appears at about 1.8 Å in all spectra, and the other features shown up to $\mathbf{k} \approx 2.2$ Å, are associated with the interactions between the vanadium and the surrounding oxygens, i.e., the first shell. The second intense peak, located at about 2.7 Å in the spectra, taken on the two cells with the lowest amount of inserted lithium, was assigned to a vanadium–vanadium (second shell) interaction.[30,35] The curves in A were taken on the electrodes with a Li^+/V_2O_5 ratio of ca. 1.5. The two curves, obtained from two different electrodes in two different cells, are almost identical. This indicates the reproducibility of the measurements as well. Of even more importance is the comparison between the FT plots of the discharged electrode in the pristine state (before discharge) and the charged electrode after almost complete delithiation. As seen in Fig. 8B, the shape and positions of the delithiated electrode FT peaks (dashed line) are extremely close to those for the pristine electrode. In particular, even the peaks shown at high *R* values that are due to the atoms beyond the first shell, e.g., the vanadium-vanadium interaction peak that appears at 2.8 Å, showed a marked position reversibility. Further work is in progress to perform a complete analysis of the EXAFS measurements. Nevertheless, we consider the qualitative analysis of the spectra presented here to be of great importance. Recently, Mansour et al.[36] have shown that in situ XAS measurements are a powerful tool to investigate the reversibility of the lithium insertion in intercalation compounds. The reversibility of the position of the peaks associated with atoms beyond the first shell clearly infers that there is a structural reversibility of the system beyond the first shell, i.e., and the VO_5 square-based pyramid unit. It involves a long-range reversibility that extends over the entire V_2O_5 layer.

Conclusions

Spray-coated electrodes of freeze-dried V_2O_5 xerogel showed excellent performance as lithium intercalation hosts. The material was able to reversibly insert up to about 2.5 equiv Li/V_2O_5 unit at a low rate of discharge (C/55). Even at higher rates (C/12), the material showed a very high insertion capacity of almost two Li^+. The latter corresponded to a specific capacity of more than 270 mAh/g. In addition, the high capacity was maintained upon repetitive charge/discharge cycles. The excellent electrochemical performance, both in terms of lithium host capacity and reversibility of the intercalation process, was related to the reduced layered order of the freeze-dried V_2O_5 xerogel. The enhanced amorphicity of the material allows for easier lattice expansions and contractions upon lithium intercalation without any major disruption of the V_2O_5 layer structure. The latter was confirmed by in situ XANES investigation that have demonstrated the complete reversibility of the electronic modifications induced by lithium insertion in freeze-dried V_2O_5 xerogel. A preliminary, qualitative analysis of the in situ EXAFS investigation indicates that there is long-range structural reversibility that extends beyond the VO_5 square-based pyramid unit.

Acknowledgments

The work at the University of Minnesota was supported by DOE under contract DE-FG02-93ER14384. The authors from Brookhaven

S0013-4651(98)09-048-X CCC: $7.00

National Laboratory gratefully acknowledge the support of the U.S. Department of Energy, Office of Advanced Transportation Technologies, under contract no. DE-AC02-98CH10886. The NSLS and Beam Line X11A is supported by the Department of Energy, Division of Materials Sciences, under contract no. DE-AC02-98CH10886.

The University of Minnesota assisted in meeting the publication costs of this article.

References

1. S. Passerini, A. L. Tipton, and W. H. Smyrl, *Sol. Energy Mater. Sol. Cells*, **39**, 167 (1995).
2. S. Passerini, D. Chang, X. Chu, D. B. Le, and W. Smyrl, *Chem. Mater.*, **7**, 780 (1995).
3. D. B. Le, S. Passerini, A. L. Tipton, B. B. Owens, and W. H. Smyrl, *J. Electrochem. Soc.*, **142**, L102 (1995).
4. J. Livage, *Chem. Mater.*, **3**, 578 (1991).
5. J. Lemerle, L. Nejem, and J. Lefebvre, *J. Inorg. Nucl. Chem.*, **42**, 17 (1980).
6. J. Lemerle and J. Livage, *J. Colloid and Interface Sci.*, **94**, 75 (1983).
7. J. Lemerle, P. Aldebert, N. Baffier, and J. Livage, *J. Colloid Interface Sci.*, **94**, 84 (1983).
8. G. A. Pozarnsky and M. A. McCormick, *Chem. Mater.*, **6**, 830 (1994).
9. J. J. Legendre and J. Livage, *J. Colloid Interface Sci.*, **94**, 75 (1983).
10. T. Yao, Y. Oka, and N. Yamamoto, *Mater. Res. Bull.*, **27**, 669 (1992).
11. P. Aldebert, N. Baffier, N. Gharbi, and J. Livage, *Mater. Res. Bull.*, **16**, 669 (1981).
12. N. Abello, E. Husson, Y. Repelin, and G. Lucazeau, *J. Solid State Chem.*, **56**, 379 (1985).
13. R. Baddour, J. P. Pereira, R. Messina, and L. Perichon, *J. Electroanal. Chem.*, **314**, 81 (1991).
14. H. K. Park and W. H. Smyrl, *J. Electrochemi. Soc.*, **141**, L25 (1994).
15. K. West, B. Zachau-Christiansen, T. Jacobsen, and S. Skaarup, *Electrochim. Acta*, **38**, 1215 (1976).
16. E. Prouzet, C. Cartier, F. Villain, and J. Tranchant, *J. Chem. Soc., Faraday Trans.*, **92**, 103 (1996).
17. S. Passerini, D. B. Le, H. C. Foong, B. B. Owens, and W. H. Smyrl, in *Rechargeable Lithium and Lithium Ion (RCT) Batteries*, S. Megahed, B. M. Barnett, and L. Xie, Editors, PV 94-28, p. 297, The Electrochemical Society Proceedings Series, Pennington, NJ (1995).
18. S. Passerini, W. H. Smyrl, M. Berrettoni, R. Tossici, M. Rosolen, R. Marassi, and F. Decker, *Solid State Ionics*, **90**, 5 (1996).
19. J. McBreen and S. Mukerjee, *J. Electrochem. Soc.*, **142**, 3399 (1995).
20. J. McBreen, S. Mukerjee, X. Q. Yang, T. R. Thurston, and N. M. Jisrawi, in *Second International Symposium on New Materials for Fuel Cells and Modern Battery Systems*, O'Savadogo, and P. R. Roberge, Editors, Ecole Polytechnique, Montreal, p. 348c, July 6-10 (1997).
21. L. H. Manhart, in *Instructions for Composite Cathode Processing; Pellets, Casts, Spray Coating; Coin and Bag Cells*; Corrosion Research Center, Chemical Engineering and Materials Science Department, University of Minnesota, Minneapolis, MN (1998).
22. J. Wong, F. W. Lyte, R. P. Messmer, and D. H. Maylotte, *Phys. Rev. B*, **30**, 5596 (1984).
23. A. L. Tipton, S. Passerini, B. B. Owens, and W. H. Smyrl, *J. Electrochem. Soc.*, **143**, 3473 (1996).
24. P. P. Prosini, S. Passerini, R. Vellone, and W. H. Smyrl, *J. Power Sources*, **75**, 73 (1998).
25. F. Coustier, S. Passerini, and W. H. Smyrl, *Solid State Ionics*, **100**, 247 (1997).
26. P. E. Stallworth, S. Kostov, M. L. denBoer, S. G. Greenbaum, and C. Lampe-Onnerud, *J. Appl. Phys.*, **83**, 1247 (1998).
27. A. Bianconi, E. Fritish, G. Calais, and J. Petiau, *Phys. Rev. B*, **32**, 4292 (1985).
28. G. Bunker and E. A. Stern, *Phys. Rev. Lett.*, **52**, 1990 (1984).
29. S. Stizza, M. Benfatto, A. Bianconi, J. Garcia, G. Mancini, and C. R. Natoli, *J. Phys.*, **C8**, 691 (1986).
30. S. Stizza, G. Mancini, M. Benfatto, C. R. Natoli, J. Garcia, and A. Bianconi, *Phys. Rev. B*, **40**, 12229 (1989).
31. R. Tossici, R. Marassi, M. Berrettoni, S. Stizza, and G. Pistoia, *Solid State Ionics*, **57**, 227 (1992).
32. R. Tossici, R. Marassi, M. Berrettoni, S. Stizza, and G. Pistoia, *Solid State Ionics*, **67**, 77 (1993).
33. D. E. Clinton, D. A. Tryk, I. T. Bae, F. L. Urbach, M. R. Antonio, and D. A. Scherson, *J. Phys. Chem.*, **100**, 18511 (1996).
34. S. Passerini, D. B. Le, W. H. Smyrl, M. Berrettoni, R. Tossici, R. Marassi, and M. Giorgetti, *Solid State Ionics*, **104**, 195 (1997).
35. C. Cartier, A. Tranchant, M. Verdaguer, R. Messina, and H. Dexpert, *Electrochim. Acta*, **35**, 889 (1990).
36. A. N. Mansour, S. Mukerjee, X. Q. Yang, and J. McBreen, Abstract 105, The Electrochemical Society Meeting Abstracts, Vol. 98-2, Boston, MA, Nov 1-6, 1998.